ELSEVIER

Contents lists available at ScienceDirect

Science Bulletin

journal homepage: www.elsevier.com/locate/scib



Article

Zonal mean and shift modes of historical climate response to evolving aerosol distribution

Sarah M. Kang a,*, Shang-Ping Xie b, Clara Deser c, Baoqiang Xiang d,e

- ^a School of Urban and Environmental Engineering, Ulsan National Institute of Science and Technology, Ulsan 44919, Republic of Korea
- ^b Scripps Institution of Oceanography, University of California San Diego, La Jolla CA 92093, USA
- ^c Climate and Global Dynamics Division, National Center for Atmospheric Research, Boulder CO 80307, USA
- ^d National Oceanographic and Atmospheric Administration/Geophysical Fluid Dynamics Laboratory, Princeton NJ 08540, USA
- ^e University Corporation for Atmospheric Research, Boulder CO 80307, USA

ARTICLE INFO

Article history: Received 27 May 2021 Received in revised form 13 June 2021 Accepted 15 June 2021 Available online 13 July 2021

Keywords:
Aerosol forced response
Aerosol increase mode
Aerosol shift mode
Energetics
Coupled atmosphere-ocean coupling
Hierarchical modeling

ABSTRACT

Anthropogenic aerosols are effective radiative forcing agents that perturb the Earth's climate. Major emission sources shifted from the western to eastern hemisphere around the 1980s. An ensemble of single-forcing simulations with an Earth System Model reveals two stages of aerosol-induced climate change in response to the global aerosol increase for 1940–1980 and the zonal shift of aerosol forcing for 1980–2020, respectively. Here, using idealized experiments with hierarchical models, we show that the aerosol increase and shift modes of aerosol-forced climate change are dynamically distinct, governed by the inter-hemispheric energy transport and basin-wide ocean-atmosphere interactions, respectively. The aerosol increase mode dominates in the motionless slab ocean model but is damped by ocean dynamics. Free of zonal-mean energy perturbation, characterized by an anomalous North Atlantic warming and North Pacific cooling, the zonal shift mode is amplified by interactive ocean dynamics through Bjerknes feedback. Both modes contribute to a La Niña-like pattern over the equatorial Pacific. We suggest that a global perspective that accommodates the evolving geographical distribution of aerosol emissions is vital for understanding the aerosol-forced historical climate change.

© 2021 Science China Press. Published by Elsevier B.V. and Science China Press. All rights reserved.

1. Introduction

Anthropogenic aerosols mask a considerable fraction of greenhouse warming through scattering and absorbing shortwave radiation and altering microphysical and radiative properties of clouds [1–3]. In contrast to well-mixed greenhouse gases, anthropogenic aerosols are geographically distributed because of localized emission sources and the short atmospheric residence time. Spatial inhomogeneity of anthropogenic aerosol forcing leads to distinct regional responses in the hydrological cycle through changes in large-scale atmospheric circulation. For example, anthropogenic aerosols during the second half of the 20th century are suggested to have caused a southward shift of the zonal-mean intertropical convergence zone (ITCZ) with a peak in the 1980s [2–4], a weakening of the South Asian summer monsoon [5] and the north drying and south wetting trends in eastern China since the 1950s [6], and

the prolonged drought and a partial recovery in the African Sahel before and after 1980, respectively [7,8].

Global emissions of anthropogenic aerosols steadily increased through the 20th century. Previous studies have emphasized the effects of this global increase in aerosol forcing, often in comparison with greenhouse warming [9]. Around the 1980s, anthropogenic aerosol sources shifted from the western hemisphere to the eastern hemisphere (Fig. S1 online) as aerosol emissions from North America and Europe have declined due to air quality regulations while emissions from Asia have continued to increase [10]. A large ensemble of single-forcing simulations with the Community Earth System Model version 1 (denoted CESM1 LE AER; Materials and methods) reveals a two-stage evolution of aerosol-induced climate change [11]: the aerosol forcing from 1940 to 1980 has produced a general Northern Hemisphere cooling except over a small area in the subpolar North Atlantic (Fig. 1b; [12]) while from 1980 to 2020, it has caused the North Pacific to cool and the North Atlantic to warm (Fig. 1c). The distinct sea surface temperature (SST) response pattern gives rise to distinct precipitation responses, including a decrease in Asian monsoon rainfall throughout the late

^{*} Corresponding author.

E-mail address: skang@unist.ac.kr (S.M. Kang).

S.M. Kang et al. Science Bulletin 66 (2021) 2405–2411

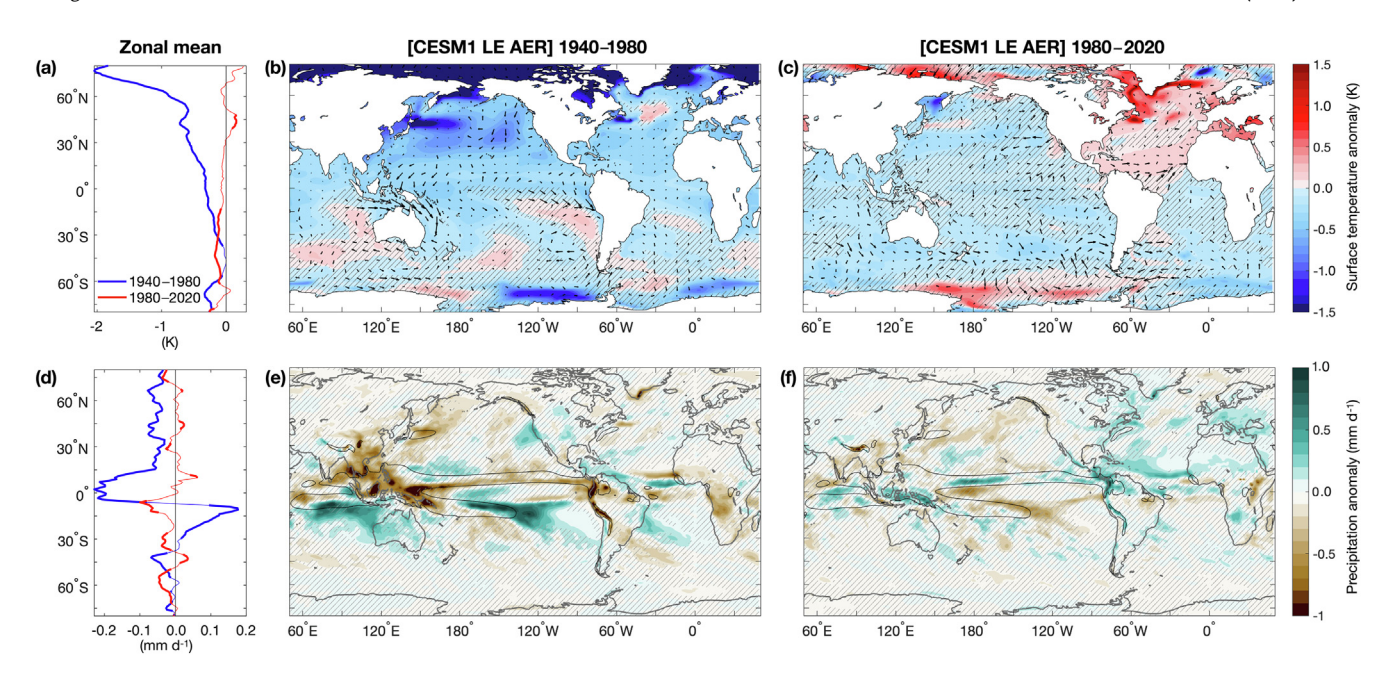


Fig. 1. (a) Zonal- and ensemble-mean linear trends of surface temperature between 1940 and 1980 (blue) and 1980–2020 (red), with the significant responses at the 95% confidence level based on a two-sided t-test in thicker lines, and spatial map of linear trends in SST (colors) and horizontal wind vectors at 850 hPa for the period between (b) 1940–1980 and (c) 1980–2020 from CESM LE aerosol single-forcing simulations. (d–f) same as (a–c) but for precipitation. The black contours in (e) and (f) show the 6 mm d⁻¹ isopleth of the precipitation climatology between 1920 and 2005 from the control LE ALL simulation (see Materials and methods). Hatched regions indicate statistically insignificant values at the 95% confidence level based on a two-sided t-test.

20th century [13] and Sahel drought until the 1980s and the recovery afterward [11,14,15] (Fig. 1e, f).

To illustrate the effect of a zonal shift in aerosol forcing, here we conduct a set of idealized experiments, where the insolation is reduced at different longitudes to mimic the regional aerosol forcing (Fig. S2 online). The radiative cooling over Asia represents the eastern hemisphere aerosol forcing and that over North America and Europe represents the western hemisphere aerosol forcing. We emphasize that our experiments are not intended to reproduce every detail of the aerosol-forced climate response but rather to highlight important governing dynamics. Specifically, we keep the radiative cooling in the eastern and western hemispheres of the same magnitude and in the same latitudinal band so the zonal shift mode is free of zonal-mean energy perturbations. The average of the eastern and western hemisphere radiative cooling (aerosol increase mode hereafter) mimics the concurrent increase of aerosols over Asia, North America, and Europe during 1940-1980 while the difference (aerosol shift mode) mimics the aerosol increase in Asia and decline in the western hemisphere during 1980-2020. We show that the two modes not only capture the distinct evolution of aerosol-forced climate response in CESM1 LE AER but also are governed by distinct coupled dynamics. The aerosol increase mode involves a marked response in ocean-atmospheric overturning circulation across the equator to balance the strong zonal-mean energy perturbation, while the aerosol shift mode is not subject to a zonal-mean energy perturbation and is rather shaped by basin-scale coupled ocean-atmosphere dynamics. To isolate the role of interactive ocean dynamics, we utilize a hierarchy of models by applying the same perturbation to an atmospheric general circulation model coupled to either a slab ocean model (SOM) or a dynamic ocean model (DOM).

2. Materials and methods

The aerosol-forced climate trends during the two periods of the historical period, 1940–1980 vs. 1980–2020, are obtained by contrasting the Community Earth System Model version 1 (CESM1)

Large-Ensemble (LE) all-forcing simulations (ALL) [16] with the recently performed CESM1 LE aerosol single-forcing simulations, which use the same forcing protocol as ALL except one forcing agent that is held fixed at 1920 conditions [11]. There are a 20member ensemble with fixed industrial aerosols (XAERind) and a 15-member ensemble with fixed biomass-burning aerosols (XAERbmb). The aerosol-forced response is computed by summing the contributions of both types of aerosols, which is obtained as the difference between the ensemble-mean of XAERind (or XAERbmb) from the ensemble-mean of ALL. The linear trends are based on least-squares regression analysis. Since the idealized experiments are conducted with the Geophysical Fluid Dynamics Laboratory (GFDL) model, we contrast CESM1 LE with the aerosol single-forcing simulations from GFDL CM3, which are integrated up to 2005 with three members [17]. The global surface temperature trend is correlated in space at 0.81 between 1940 and 1980 while the pattern correlation drops to 0.06 between 1980 and 2005 (Fig. S3 online). The precipitation trend between 30°S and 30°N is correlated at 0.34 and 0.01 for the respective period (Fig. S4 online). The lower pattern correlations for precipitation compared to temperature are likely a result of model differences in precipitation mean state, different treatments of aerosol microphysics, and small signal-to-noise for the GFDL ensemble. The lower pattern correlations for the later period (1980-2005) compared to the earlier period (1940–1980) may reflect the shorter time interval and thus small signal-to-noise.

We conduct the idealized experiments with the developmental version of the GFDL Atmospheric Model version 4 (AM4) [18] coupled with the ocean model used in GFDL Forecast-Oriented Low Ocean Resolution model [19]. Both the atmospheric and oceanic models have an approximate 1° horizontal resolution. The atmospheric model has 32 vertical levels and the oceanic model has 50 vertical levels. The experiments are designed to probe the coupled ocean–atmosphere response to a zonal shift in radiative cooling from the western to eastern hemisphere. The equilibrated pre-industrial simulation is perturbed by reducing insolation by 0.4 PW between 45° and 65°N confined to a limited domain over

S.M. Kang et al. Science Bulletin 66 (2021) 2405–2411

Asia or North America or Europe, which amounts to 67 W m⁻² when averaged over the forcing region (Fig. S2 online). While net radiation response to aerosol forcing is of order 10 W m⁻² at a regional scale [20], we perturb the system with a stronger forcing to allow for a clear estimation of the forced response. The eastern hemisphere aerosol forcing is represented by the northern extratropical Asian radiative cooling while the western hemisphere aerosol forcing is represented by the average of North American and European radiative cooling. While European anthropogenic aerosol emissions are indeed located at high latitudes around 45°-65°N (Fig. S1 online), the Asian and North American forcing are prescribed at rather higher latitudes than the actual aerosol emission regions to separate remote extratropical impacts from local tropical impacts on the tropical precipitation response. The average of the climate response to the eastern and western hemisphere radiative cooling defines the aerosol increase mode whereas the difference defines the aerosol shift mode. We choose to reduce insolation rather than perturbing aerosol emissions to constrain the forcing magnitude. Although the cloud response is likely to depend on the forcing type, perturbing aerosol emissions would offer a similar picture to our insolation-reduced experiments as the same interhemispheric asymmetry in aerosol-induced cooling and the ITCZ shift are driven by the total aerosol effects (i.e., direct, semidirect and indirect effects) [3]. Identical experiments are also performed using GFDL AM4 coupled to a slab ocean model (SOM) with a 50 m mixed layer depth, which only includes a thermodynamic ocean-atmospheric coupling while full ocean dynamics is absent. All perturbed experiments are integrated for 100 years after an abrupt reduction of solar flux and the annual-mean responses for the last 70 years are analyzed.

3. Results

The SST responses for the aerosol increase and shift modes in DOM (Fig. 2b, c) broadly compare well with the aerosol forced

responses in 1940-1980 and 1980-2020 (Fig. 1b, c), respectively. The aerosol forced SST response in the former period is correlated in space with the aerosol increase mode at 0.70 between 45°S and 45°N (Figs. 1b and 2b) while the aerosol shift mode is correlated with the latter period response at 0.42 (Figs. 1c and 2c). The similarity is remarkable considering model differences and a considerable idealization of experiment design. The aerosol increase mode is associated with a pronounced northern extratropical cooling (Fig. 2a, b) whereas the aerosol shift mode induces a North Pacific cooling and a North Atlantic warming (Fig. 2c) with a negligible zonal-mean response (Fig. 2a). Associated with the similar SST response pattern, the precipitation response also exhibits a large degree of similarity in spatial distribution between the idealized DOM experiments and the CESM1 LE AER (compare Fig. 3b, c with Fig. 1e, f). The pattern correlation of tropical precipitation response between 15°S and 15°N amounts to 0.58 between the aerosol increase mode and the aerosol forced response in the former period while the aerosol shift mode is correlated at 0.43 with the aerosol forced response in the latter period. Notably, our idealized experiments capture the evolving precipitation trends over the tropical Pacific and Sahel in the aerosol single-forcing simulations.

3.1. Energetic constraints on the aerosol increase mode

The aerosol increase mode is dominated by an interhemispheric structure that is largely zonally symmetric, with a more pronounced cooling in the Northern than the Southern Hemisphere (Fig. 2a, b). The eastern and western hemisphere forcings share a common zonally averaged response despite the difference in their longitudinal locations, as implied by the small zonal mean component in the aerosol shift mode. The common zonal mean component closely resembles the response to a zonally uniform radiative cooling (Fig. S5 online). The robustness of aerosol increase mode is further confirmed by a strong correlation in the climate response pattern of any two pairs of three regional cooling

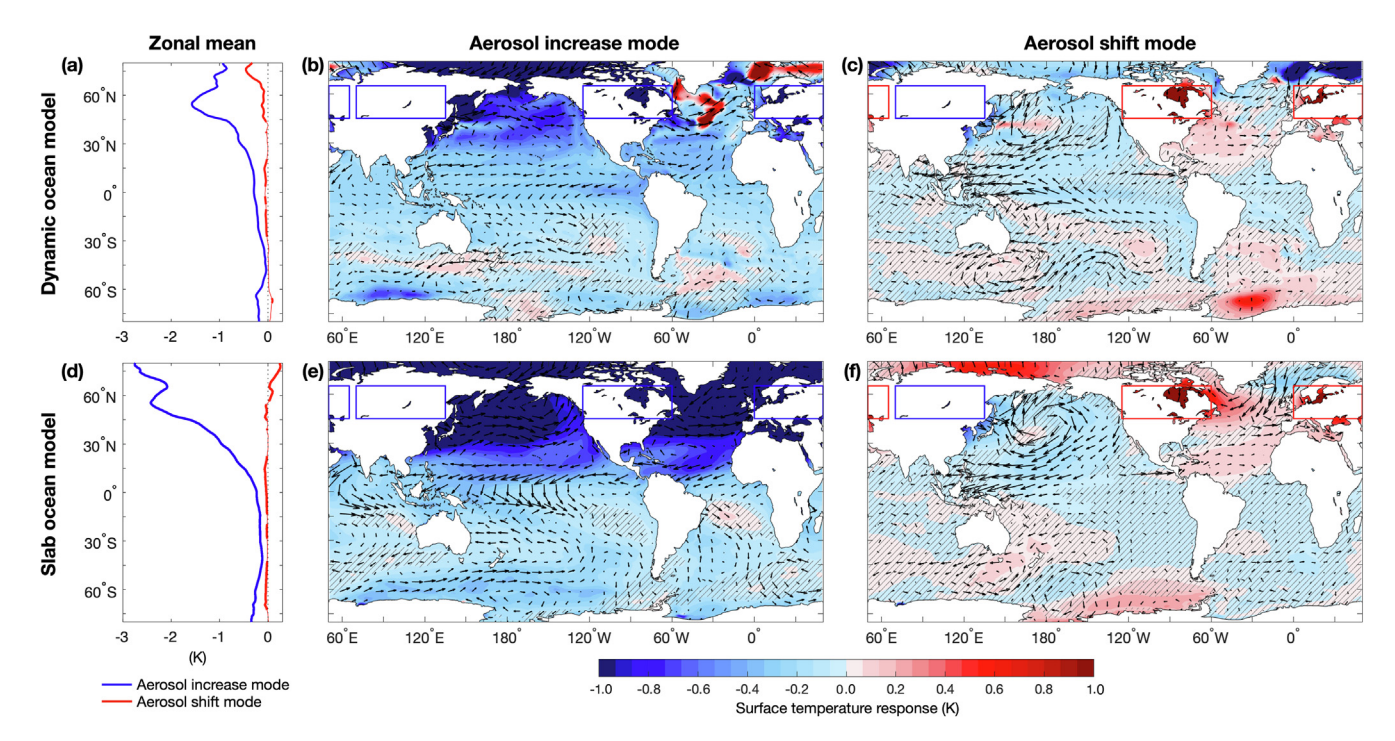


Fig. 2. (a) Zonal-mean surface temperature anomalies for the aerosol increase (blue) and shift (red) modes, with the significant responses at the 95% confidence level based on a two-sided t-test in thicker lines, and spatial pattern of SST anomalies (colors) and horizontal wind vectors at 850 hPa for (b) aerosol increase mode and (c) aerosol shift mode, from the idealized experiments with a dynamic ocean model (DOM). (d–f) same as (a–c) but for slab ocean model (SOM) experiments. Hatched regions indicate statistically insignificant values at the 95% confidence level based on a two-sided t-test.

S.M. Kang et al. Science Bulletin 66 (2021) 2405-2411

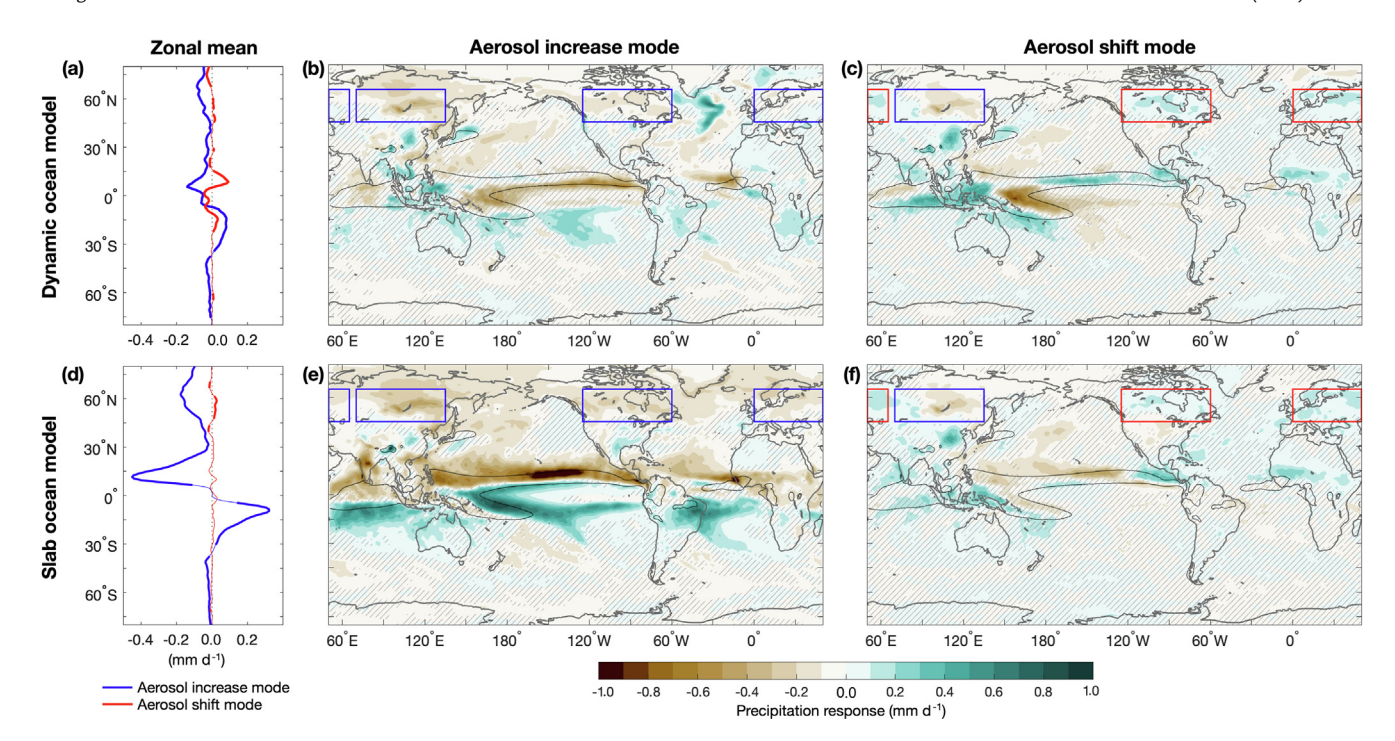


Fig. 3. (a) Zonal-mean precipitation anomalies for the aerosol increase (blue) and shift (red) modes, with the significant responses at the 95% confidence level based on a two-sided t-test in thicker lines, and spatial pattern of precipitation anomalies for aerosol increase mode (b) and aerosol shift mode (c), from the idealized experiments with a dynamic ocean model (DOM). (d, e, f) same as (a, b, c) but for slab ocean model (SOM) experiments. The black contours in the maps show the 6 mm d⁻¹ isopleth of the precipitation climatology from the preindustrial control simulation. Hatched regions indicate statistically insignificant values at the 95% confidence level based on a two-sided t-test.

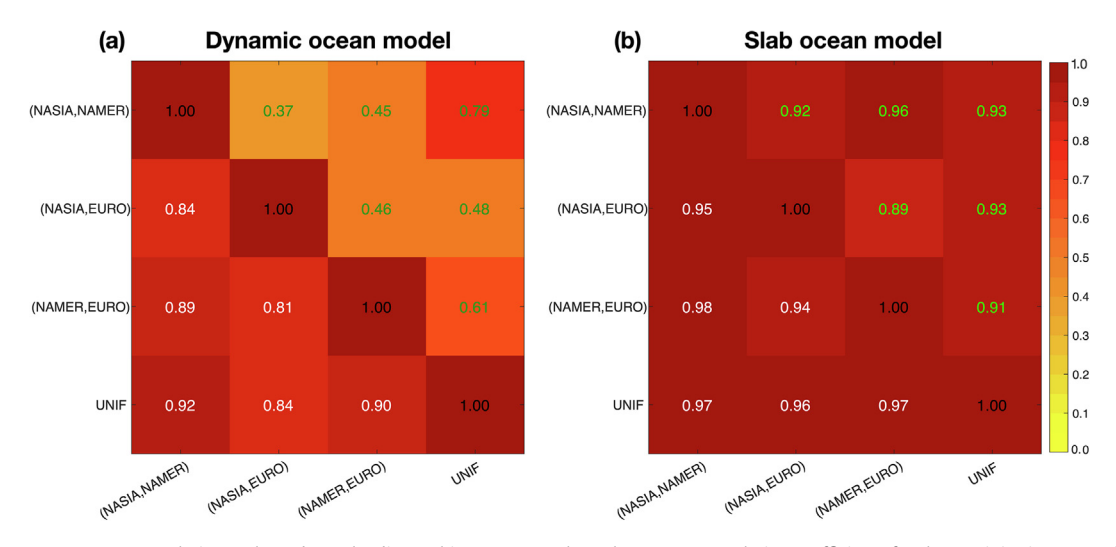


Fig. 4. Climate response pattern correlation. Values above the diagonal in green text show the pattern correlation coefficients for the precipitation anomalies over 30°S and 30°N between any two pairs of three regional cooling experiments as well as the zonally uniform forcing experiment (UNIF). Same for values below the diagonal in white text except for the surface temperature anomalies. (a) is for dynamic ocean model (DOM) and (b) is for slab ocean model (SOM) experiments.

experiments as well as the zonally uniform forcing experiment (Fig. 4).

The results from the motionless SOM (Figs. 2e and 3e) illustrate the origin of the zonal-mean energetics mode. In SOM, the climate response pattern is essentially independent of the forcing distribution (Fig. 4b). Localized cooling over the continents is advected eastward by climatological westerlies and midlatitude eddies [21,22], resulting in highly zonally symmetric temperature responses in the extratropics. The prevalent cooling of the Northern Hemisphere requires the atmosphere to transport energy from the Southern to Northern Hemisphere by anomalous Hadley circu-

lation (Fig. S6a, b online) [23,24]. This energetics constraint dictates the aerosol increase mode with a southward displacement of the zonal-mean ITCZ (Fig. 3d).

A dynamic ocean damps the aerosol increase mode. The ocean adjustment contributes about 40 % more than the atmosphere to the cross-equatorial northward energy transport to balance the reduced solar radiation in the mid-latitude Northern Hemisphere in the aerosol increase mode in DOM (Fig. 5e). In response to the intensified (weakened) trade winds in the North (South) Pacific (Fig. 2b, e), an anomalous shallow overturning cell develops (Fig. 5a) with a northward heat transport across the equator

S.M. Kang et al. Science Bulletin 66 (2021) 2405–2411

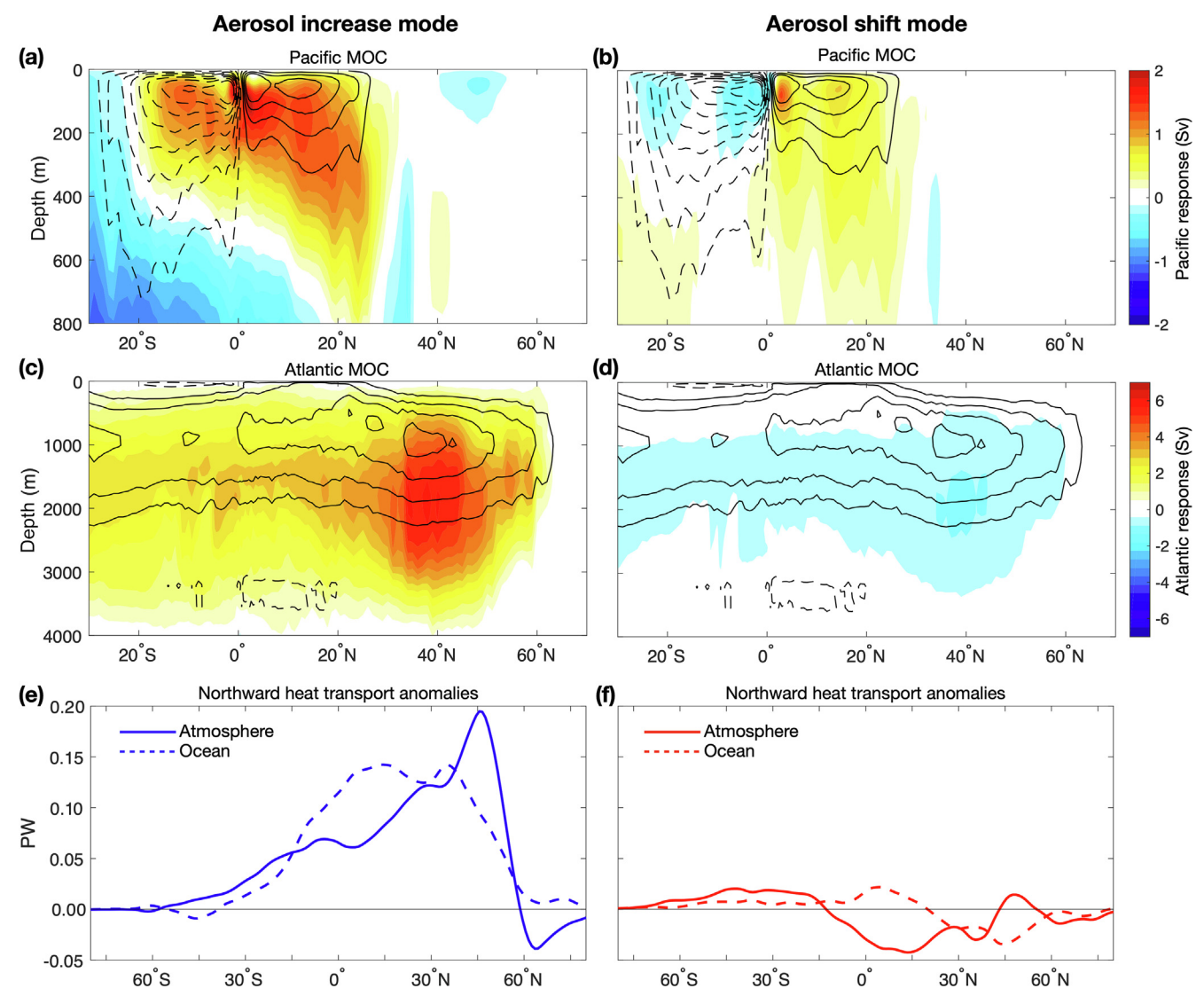


Fig. 5. Ocean meridional overturning circulation anomalies in the Indo-Pacific for aerosol increase mode (a) and aerosol shift mode (b) from the idealized experiments with a dynamic ocean model (DOM). (c, d) same as (a, b) but for the Atlantic sector. The contours show the climatology from the preindustrial control simulation. Positive values (red shading and solid contours) indicate a clockwise circulation and negative values (blue shading and dashed contours) indicate a counter-clockwise circulation. Northward energy transport response in aerosol increase mode (e) and aerosol shift mode (f). The solid line indicates the atmospheric moist static energy transport response, which is indirectly calculated from the net top-of-atmosphere radiation and net surface energy fluxes. The dashed line indicates the implied oceanic energy transport response, which is calculated as the latitudinal integral of net surface energy flux response.

[25,26]. The deep Atlantic Meridional Overturning Circulation (AMOC) strengthens (Fig. 5c) as the surface cooling and increased salinity, from reduced precipitation and less freshwater input from Arctic sea ice, make the surface waters in the North Atlantic denser, enhancing the deep water formation in the Labrador Sea. The strengthened ocean meridional overturning circulation induces anomalously northward heat transport (Fig. 5e), reducing the meridional SST gradients across the equator (Fig. 2a, d). This is consistent with a weaker Hadley circulation response (Fig. S6a, b online), a reduced ITCZ shift (Fig. 3a, d), and less significant Sahel rainfall response (Fig. 3b, e) in DOM compared to SOM [27]. Our DOM experiment exhibits a rather small Sahel drying response (Fig. 3b), as compared to earlier studies attributing the Sahel drought in the 1970s and 1980s partly to aerosol forcing [2,8,28]. This is possibly because the North American radiative cooling is prescribed at higher latitudes than the actual radiative forcing with a peak around 30°N.

3.2. Positive ocean dynamical feedback in the zonal shift mode

Now we proceed to discuss the aerosol shift mode, which is related to the aerosol-forced climate responses since the 1980s. The aerosol shift mode features strong zonal variations between the North Pacific cooling and the North Atlantic warming (Fig. 2c), with a negligible zonal-mean surface temperature response (Fig. 2a). Cold advection from Asia produces cold anomalies over the North Pacific, intensifying the climatological northeasterlies over the subtropical North Pacific. The associated anomalous anticyclonic atmospheric circulation over the midlatitude North Pacific is present in both DOM and SOM (Fig. 2c, f). Then, the North Pacific cooling is propagated southwestward via wind-evaporation-SST (WES) feedback [29] (Fig. 2c, f). Hence, the extratropical surface cooling reaches the equatorial Pacific through the central to the western basin, resulting in anomalous easterlies in the western equatorial Pacific (Fig. 2f). When coupled

S.M. Kang et al. Science Bulletin 66 (2021) 2405-2411

to a dynamic ocean model, these strengthened easterly trades lead to a strengthening of the shallow overturning circulation in the Pacific (Fig. 5b), intensifying cold upwelling along the equator, thereby driving a La Niña-like cooling pattern (Fig. 2c). A cooling of the water subducted in the northern subtropical cell would also contribute to La Niña-like Pacific cooling by reducing the temperature of water that is upwelled in the equatorial Pacific [30,31]. The equatorial Pacific cooling is amplified through Bjerknes feedback in DOM, featuring a westward shift of western Pacific deep convective activity, a drier equatorial Pacific and a wetter northern ITCZ (Fig. 3c) [32]. This positive ocean dynamical feedback explains a more prominent aerosol shift mode in DOM than SOM, which is particularly evident from the precipitation response in the tropical Pacific (Fig. 3c, f). This, together with the ocean dynamic damping of the aerosol increase mode, makes the contributions from the two modes comparable to tropical precipitation change, both in the zonal mean and variation (Fig. 3).

Over the North Atlantic, the reduction in aerosols from North America produces warm anomalies, which propagate southwestward with the weakened easterlies (Fig. 2c, f). The AMOC slightly weakens with a warming and freshening North Atlantic (Fig. 5d), damping the North Atlantic warming in DOM compared with SOM (Fig. 2c, f). As a result, a northward Atlantic ITCZ displacement is clearer in SOM (Fig. 3c, f). Small tropical Atlantic precipitation response in DOM is possibly because of our idealized experiment design as the radiative forcing is prescribed at too high latitudes compared to the realistic aerosol forcing and the western and eastern hemisphere forcing magnitude is constrained to be same but differs in reality. However, the accompanying increase in Sahel rainfall is evident regardless of the presence of ocean dynamics, implying that the observed recovery of Sahel drought in the recent decades may be partially attributable to a zonal shift in aerosol forcing [11,33]. This is a different perspective for understanding the Sahelian precipitation recovery in the recent decades from the previous argument that emphasizes the direct atmospheric response to greenhouse gases [34].

4. Discussion

Our idealized experiments offer dynamical insights into the global climate response to aerosol forcing. We show that the aerosolforced climate change in the historical period can be largely decomposed into aerosol increase and shift modes that originate in the extratropics. The aerosol increase mode dominates the period with a global increase in aerosol emissions from the 1940s to 1980s, with the predominant zonal-mean component that is governed by the energetics framework. The framework predicts a differential cooling in the Northern Hemisphere and a southward displaced zonal-mean ITCZ [35]. By contrast, the aerosol shift mode is important for the period since the 1980s when the aerosol forcing has shifted zonally from North America and Europe to Asia and hence the tropical climate response pattern is distinct between the Pacific and Atlantic basins. Consequently, the aerosol increase mode is robust and not sensitive to the forcing distribution (Fig. 4) while the aerosol shift mode is dependent on the forcing profile such as relative location and magnitude.

Our hierarchical modeling approach allows us to reveal the distinct role of ocean dynamics in modulating the two modes as summarized in Fig. 6. In the absence of ocean dynamics, the aerosol increase mode is dominant with a robust zonally symmetric structure while the aerosol shift mode is insignificant associated with zero zonal-mean radiative forcing. However, the aerosol increase mode is preferentially damped by ocean dynamical adjustments (Fig. 3b, e), consistent with the energetics framework as has emerged in recent literature [25,27,36]. Conversely, the aerosol

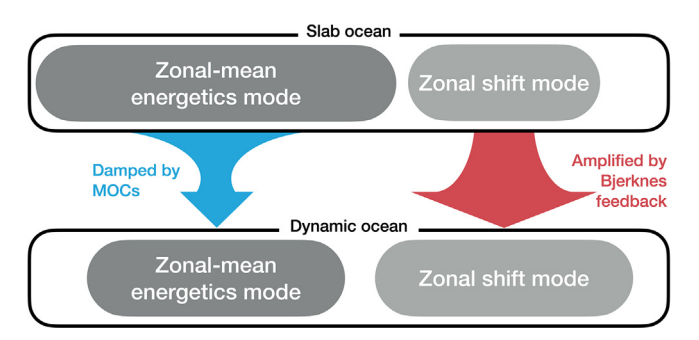


Fig. 6. Schematic of distinctive dynamics governing the two modes. In slab ocean model, the zonal-mean mode, which is explained by the energetics framework, dominates the zonal shift mode. Ocean dynamical adjustments preferentially damp the zonal-mean mode while amplifying the zonal shift mode via Bjerknes feedback. Consequently, the two modes are comparably important in dynamic ocean model.

shift mode is amplified by coupled ocean-atmosphere dynamics, especially Bierknes feedback on the equator. As a consequence. the two modes become comparably important in DOM, but with a distinct spatial pattern (Fig. 3b, c): the aerosol increase mode induces a southward displacement of the tropical precipitation while the aerosol shift mode causes a westward shift of the western Pacific precipitation, a drier equatorial Pacific and a wetter northern ITCZ. Although the two modes induce a distinct tropical precipitation response, they share a common La Niña-like cooling pattern over the equatorial Pacific (Fig. 2b, c). The results suggest that the persistent aerosol-forced North Pacific cooling may have contributed to the observed La Niña-like cooling of the equatorial Pacific in the recent decades [37,38]. We propose that the evolving spatial distribution of aerosol forcing needs to be considered in interpreting the multidecadal variability of tropical climate. As aerosol emissions in Asia eventually decrease in the future, it would induce a climate response opposite to the aerosol increase mode, boosting the greenhouse warming and reorganizing rainfall patterns around the world.

Our radiative forcing is highly idealized, with a theoretical appeal that keeps the zonal shift mode free of zonal-mean energy perturbations. By confining the radiative perturbations north of 45°N, we show that marked climate response penetrates deep into the tropics as required by interhemispheric energy transport and/ or through coupled ocean-atmospheric feedbacks. More realistic distributions of aerosol forcing would certainly improve the realism of simulated climate response on local to regional scales, especially around major emission sources. For example, our idealized experiments fail to reproduce the drying trends over South Asia since the 1940s (Fig. 3), which are primarily driven by local aerosol emissions [14,39,40]. Also, our aerosol increase mode (Fig. 3b) does not capture the early period drying over South America and Central Africa (Fig. 1e), a change for which the tropical biomass burning aerosol forcing is important (Fig. S1a online). Despite these caveats, a global perspective of large-scale coupled ocean-atmospheric adjustments to the spatio-temporal evolution of aerosol forcing as presented here provides a conceptual framework for explaining aerosol-forced climate change during the historical period.

Conflict of interest

The authors declare that they have no conflict of interest.

Acknowledgments

Sarah M. Kang was supported by the Basic Science Research Program through the National Research Foundation of Korea (NRF) funded by the Ministry of Science, ICT and Future Planning S.M. Kang et al. Science Bulletin 66 (2021) 2405-2411

(2016R1A1A3A04005520 and 2017K2A9A1A06056874). Shang-Ping Xie was supported by the National Science Foundation (AGS-1934392). The Community Earth System Model project is supported primarily by the National Science Foundation (NSF). This work was based upon work supported by the National Center for Atmospheric Research, which is a major facility sponsored by the NSF under Cooperative Agreement (1852977). Computing and data storage resources, including the Cheyenne supercomputer (doi: 10.5065/D6RX99HX), were provided by the Computational and Information Systems Laboratory (CISL) at National Center for Atmospheric Research.

Author contributions

Sarah M. Kang and Shang-Ping Xie conceived the research. Sarah M. Kang, Shang-Ping Xie, and Baoqiang Xiang designed and performed the idealized experiments. Clara Deser provided the CESM1 LE AER data. All authors contributed to the discussion of the results and the writing of the manuscript.

Appendix A. Supplementary materials

Supplementary materials to this article can be found online at https://doi.org/10.1016/j.scib.2021.07.013.

References

- [1] Ramanathan V, Crutzen PJ, Kiehl JT, et al. Aerosols, climate, and the hydrological cycle. Science 2001;294:2119–24.
- [2] Rotstayn LD, Lohmann U. Tropical rainfall trends and the indirect aerosol effect. | Clim 2002;15:2103-16.
- [3] Ming Y, Ramaswamy V. Nonlinear climate and hydrological responses to aerosol effects. | Clim 2009;22:1329–39.
- [4] Hwang Y-T, Frierson DMW, Kang SM. Anthropogenic sulfate aerosol and the southward shift of tropical precipitation in the late 20th century. Geophys Res Lett 2013;40:2845–50.
- [5] Bollasina MA, Ming Y, Ramaswamy V. Anthropogenic aerosols and the weakening of the South Asian summer monsoon. Science 2011;334:502–5.
- [6] Li Z, Lau WKM, Ramanathan V, et al. Aerosol and monsoon climate interactions over Asia. Rev Geophys 2016;54:866–929.
- [7] Dong B, Sutton RT, Highwood E, et al. The impacts of European and Asian anthropogenic sulfur dioxide emissions on Sahel rainfall. J Clim 2014;27:7000–17.
- [8] Ackerley D, Booth BBB, Knight SHE, et al. Sensitivity of twentieth-century Sahel rainfall to sulfate aerosol and CO₂ forcing, J Clim 2011;24;4999–5014.
- [9] Xie S-P, Lu B, Xiang B. Similar spatial patterns of climate responses to aerosol and greenhouse gas changes. Nat Geosci 2013;6:828–32.
- [10] Lamarque J-F, Bond TC, Eyring V, et al. Historical (1850–2000) gridded anthropogenic and biomass burning emissions of reactive gases and aerosols: methodology and application. Atmos Chem Phys 2010;10:7017–39.
- [11] Deser C, Phillips AS, Simpson IR, et al. Isolating the evolving contributions of anthropogenic aerosols and greenhouse gases: a new CESM1 large ensemble community resource. J Clim 2020;33:7835–58.
- [12] Dagan G, Stier P, Watson-Parris D. Aerosol forcing masks and delays the formation of the North Atlantic warming hole by three decades. Geophys Res Lett 2020:47. e2020gl090778.
- [13] Lau WKM, Kim K-M. Fingerprinting the impacts of aerosols on long-term trends of the Indian summer monsoon regional rainfall. Geophys Res Lett 2010;37:L16705.
- [14] Undorf S, Polson D, Bollasina MA, et al. Detectable impact of local and remote anthropogenic aerosols on the 20th century changes of West African and South Asian monsoon precipitation. J Geophys Res Atmos 2018;123:4871–89.
- [15] Hirasawa H, Kushner PJ, Sigmond M, et al. Anthropogenic aerosols dominate forced multidecadal Sahel precipitation change through distinct atmospheric and oceanic drivers. J Clim 2020;33:10187–204.
- [16] Kay JE, Deser C, Phillips A, et al. The Community Earth System Model (CESM) Large Ensemble Project: a community resource for studying climate change in the presence of internal climate variability. Bull Amer Meteorol Soc 2015;96:1333–49.

[17] Wang H, Xie S-P, Liu Q. Comparison of climate response to anthropogenic aerosol versus greenhouse gas forcing: distinct patterns. J Clim 2016;29:5175–88.

- [18] Zhao M, Golaz J-C, Held IM, et al. The GFDL Global Atmosphere and Land Model AM4.0/LM4.0: 1. Simulation characteristics with prescribed SSTs. J Adv Model Earth Syst 2018;10:691–734.
- [19] Vecchi GA, Delworth T, Gudgel R, et al. On the seasonal forecasting of regional tropical cyclone activity. J Clim 2014;27:7994–8016.
- [20] Wang Y, Jiang JH, Su H. Atmospheric responses to the redistribution of anthropogenic aerosols. J Geophys Res Atmos 2015;120:9625–41.
- [21] Kang SM, Held IM, Xie S-P. Contrasting the tropical responses to zonally asymmetric extratropical and tropical thermal forcing. Clim Dyn 2014;42:2033–43.
- [22] Kang SM, Park K, Hwang Y-T, et al. Contrasting tropical climate response pattern to localized thermal forcing over different ocean basins. Geophys Res Lett 2018;45:12544–52.
- [23] Broccoli AJ, Dahl KA, Stouffer RJ. Response of the ITCZ to Northern Hemisphere cooling. Geophys Res Lett 2006;33:L01702.
- [24] Kang SM, Held IM, Frierson DMW, et al. The response of the ITCZ to extratropical thermal forcing: idealized slab-ocean experiments with a GCM. J Clim 2008;21:3521–32.
- [25] Green B, Marshall J. Coupling of trade winds with ocean circulation damps ITCZ shifts. J Clim 2017;30:4395–411.
- [26] Kang SM, Shin Y, Xie S-P. Extratropical forcing and tropical rainfall distribution: energetics framework and ocean Ekman advection. npj Clim Atmos Sci 2018;1:20172.
- [27] Kay JE, Wall C, Yettella V, et al. Global climate impacts of fixing the Southern Ocean shortwave radiation bias in the Community Earth System Model (CESM). J Clim 2016;29:21.
- [28] Biasutti M, Giannini A. Robust Sahel drying in response to late 20th century forcings. Geophys Res Lett 2006;33:L11706.
- [29] Xie S-P, Philander SGH. A coupled ocean-atmosphere model of relevance to the ITCZ in the eastern Pacific. Tellus Ser A-Dyn Meteorol Oceanol 1994;46:340–50.
- [30] Gu D, Philander SGH. Interdecadal climate fluctuations that depend on exchanges between the tropics and extratropics. Science 1997;275:805–7.
- [31] Burls NJ, Fedorov AV. What controls the mean east-west sea surface temperature gradient in the equatorial Pacific: the role of cloud albedo. J Clim 2014;27:2757–78.
- [32] Kang SM, Xie S-P, Shin Y, et al. Walker circulation response to extratropical radiative forcing. Sci Adv 2020;6:eabd3021.
- [33] Bonfils CJW, Santer BD, Fyfe JC, et al. Human influence on joint changes in temperature, rainfall and continental aridity. Nat Clim Chang 2020;10:19.
- [34] Dong B, Sutton R. Dominant role of greenhouse-gas forcing in the recovery of Sahel rainfall. Nat Clim Chang 2015;5:757–60.
- [35] Kang SM. Extratropical influence on the tropical rainfall distribution. Curr Clim Chang Rep 2020;6:24–36.
- [36] Yu S, Pritchard MS. A strong role for the AMOC in partitioning global energy transport and shifting ITCZ position in response to latitudinally discrete solar forcing in CESM1.2. | Clim 2019;32:2207–26.
- [37] L'Heureux ML, Lee S, Lyon B. Recent multidecadal strengthening of the Walker circulation across the tropical Pacific. Nat Clim Chang 2013;3:571–6.
- [38] Takahashi C, Watanabe M. Pacific trade winds accelerated by aerosol forcing over the past two decades. Nat Clim Chang 2016;6:768–72.
- [39] Westervelt DM, Conley AJ, Fiore AM, et al. Connecting regional aerosol emissions reductions to local and remote precipitation responses. Atmos Chem Phys 2018;18:12461–75.
- [40] Liu L, Shawki D, Voulgarakis A, et al. A PDRMIP multimodel study on the impacts of regional aerosol forcings on global and regional precipitation. J Clim 2018;31:4429-47.



Sarah M. Kang is an associate professor at the Department of Urban and Environmental Engineering, Ulsan National Institute of Science and Technology. She received her B.S. degree from Seoul National University, and Ph.D. degree from Princeton University. She worked as a postdoctoral fellow at Columbia University. Her research interest involves global atmospheric circulation.